


Cite this: *RSC Adv.*, 2019, 9, 37344

Co₃O₄/NiO@GQD@SO₃H nanocomposite as a superior catalyst for the synthesis of chromenpyrimidines†

Javad Safaei-Ghomi * and Zahra Omidshafiei

A three-component reaction involving aromatic aldehydes, 6-amino-1,3-dimethyluracil and 4-hydroxycoumarin was achieved in the presence of the Co₃O₄/NiO@GQD@SO₃H nanocomposite as a highly effective heterogeneous catalyst to produce chromenpyrimidines. The catalyst was characterized via FT-IR, SEM, XRD, EDS, TGA, BET and VSM. This new catalyst was demonstrated to be highly effective in the preparation of chromenpyrimidines. Atom economy, low catalyst loading, reusable catalyst, applicability to a wide range of substrates and high product yields are some of the important features of this protocol.

Received 30th July 2019
Accepted 28th October 2019

DOI: 10.1039/c9ra05896f

rsc.li/rsc-advances

1. Introduction

Chromenpyrimidines are a common scaffold in multiple bioactive compounds and possess several pharmacological properties.¹ These compounds are used as analgesic, anti-pyretic,² anti-microbial,^{3,4} anti-biofilm,⁵ anti-inflammatory,⁶ anticancer,⁷ antitubercular agents.⁸ Some other examples of pyrimidines as prominent drug molecules include uramustine, piritrexim isetionate, tegafur, floxuridine, methotrexate, trimethoprim, piromidic acid, tetroxoprim and dipyrindamole, which have high bioavailability, slow onset and prolonged effect.⁹ Chromenpyrimidines have been regarded as significant targets of organic synthesis. Therefore, the development of effective methods for the preparation of chromenpyrimidines is an attractive challenge. Several methods have been reported for the preparation of chromenpyrimidines in the presence of diverse catalysts including L-proline-derived secondary amino-thiourea,¹⁰ sulfamic acid,¹¹ Zr(HSO₄)₄,¹² L-proline,¹³ and bifunctional thiourea-based organocatalyst.¹⁴ However, some of the reported procedures have disadvantages including long reaction times, use of toxic and non-reusable catalysts and undesirable reaction conditions. Therefore, to avoid these drawbacks, the search for effective methods for the preparation of chromenpyrimidines is still desirable. Nanoparticles exhibit good catalytic activity owing to their large surface area and active sites. Metal oxides are a broad class of materials that have been researched extensively due to their unique attributes and potential applications in various fields. Graphene quantum

dots (GQDs) are a new member of the carbon nanostructure family, which have quasi-spherical structures. GQDs have gained intensive attention due to their significant features, biological,¹⁵ biomedical,¹⁶ and therapeutic applications,¹⁷ as a new class of photocatalysts¹⁸ and surfactants,¹⁹ and electrochemical biosensing,²⁰ electrocatalytic,²¹ lithium battery,²² optical and photovoltaic,²³ photoluminescence,^{24,25} bioimaging,²⁶ and catalytic applications.²⁷ The potential applications of N-graphene quantum dots were recently reviewed based on experimental and theoretical studies.^{28–31} The synthesis of highly efficient nanocomposite catalysts for the synthesis of organic compounds is still a big challenge. To obtain a larger surface area and more active sites, nanocatalysts are functionalized with active groups.^{32–34} It has been demonstrated that the decoration of nanocatalysts with GQDs prevents the aggregation of fine particles, and thus increases the effective surface area and number of reactive sites for efficient catalytic reactions. The chemical groups on GQD can catalyze chemical reactions, and their –COOH and –SO₃H groups can serve as acid catalysts for many reactions.^{27–36} Herein, we report the use of a Co₃O₄/NiO@GQD@SO₃H nanocomposite as a new efficient catalyst for the preparation of chromenpyrimidines through a three-component reaction involving aromatic aldehydes, 6-amino-1,3-dimethyluracil and 4-hydroxycoumarin (Scheme 1).

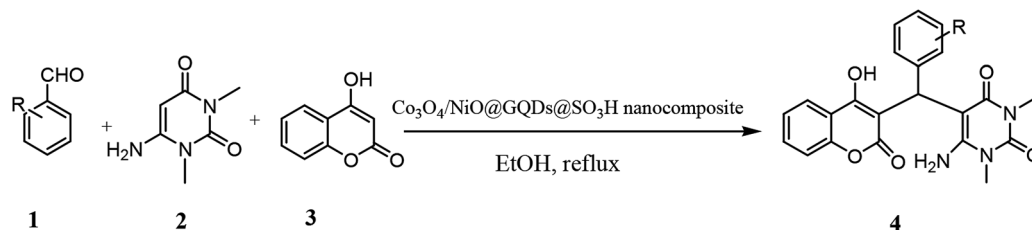
2. Results and discussion

Initially, we prepared Co₃O₄/NiO nanoparticles *via* simple techniques. A facile hydrothermal method was used for the preparation of N-GQDs.³⁷ Sulfonated graphene quantum dots were prepared using chlorosulfonic acid.³⁸ The XRD patterns of Co₃O₄/NiO, Co₃O₄/NiO@N-GQDs and Co₃O₄/NiO@GQD@SO₃H nanocomposite are shown in Fig. 1, which confirm the presence of both NiO (JCPDS No.22-1189) and Co₃O₄ (JCPDS no 65-3103).

Department of Organic Chemistry, Faculty of Chemistry, University of Kashan, Kashan, P. O. Box 87317-51167, I. R. Iran. E-mail: safaei@kashanu.ac.ir; Fax: +98-31-55912397; Tel: +98-31-55912385

† Electronic supplementary information (ESI) available. See DOI: 10.1039/c9ra05896f





Scheme 1 Synthesis of chromenpyrimidines using the $\text{Co}_3\text{O}_4/\text{NiO}@GQD@SO_3\text{H}$ nanocomposite.

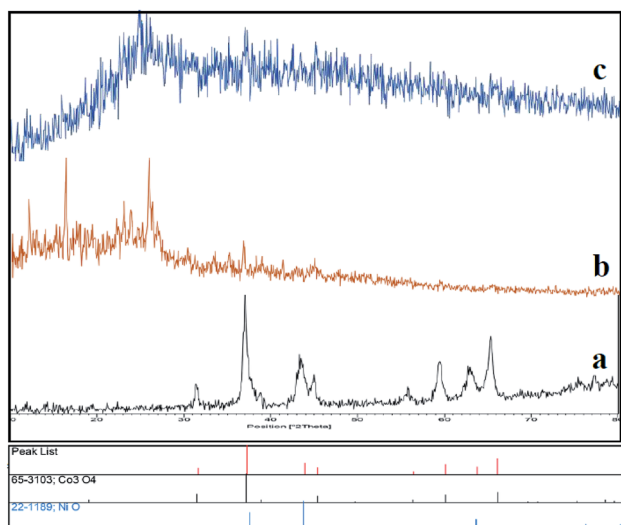


Fig. 1 XRD patterns of (a) $\text{Co}_3\text{O}_4/\text{NiO}$, (b) $\text{Co}_3\text{O}_4/\text{NiO}@GQDs$ and (c) $\text{Co}_3\text{O}_4/\text{NiO}@GQD@SO_3\text{H}$.

To investigate the morphology and particle size of the nanoparticles, SEM images of $\text{Co}_3\text{O}_4/\text{NiO}$ and $\text{Co}_3\text{O}_4/\text{NiO}@GQD@SO_3\text{H}$ nanocomposite were measured, as shown in Fig. 2. The SEM images of the $\text{Co}_3\text{O}_4/\text{NiO}@GQD@SO_3\text{H}$ nanocomposite show the formation of uniform particles, and the energy-dispersive X-ray spectrum (EDS) confirms the presence of Co, Ni, O, S and C species in the structure of the nanocomposite (Fig. 3).

The magnetic properties of the nanocomposites before and after their decoration with GQDs were tested using a vibrating-sample magnetometer (VSM) (Fig. 4). The lower magnetism of the as-synthesized $\text{Co}_3\text{O}_4/\text{NiO}@GQD@SO_3\text{H}$ compared with that of $\text{Co}_3\text{O}_4/\text{NiO}$ is ascribed to the antiferromagnetic behavior of the GQDs as a dopant. These results demonstrate that the magnetization property decreased by coating and functionalization.^{39,40}

The FT-IR spectra of $\text{Co}_3\text{O}_4/\text{NiO}$, $\text{Co}_3\text{O}_4/\text{NiO}@N\text{-GQD}$ and $\text{Co}_3\text{O}_4/\text{NiO}@GQD@SO_3\text{H}$ nanocomposite are shown in Fig. 5. The absorption peak at 3335 cm^{-1} is related to the stretching vibrational absorptions of OH. The peaks at 461.4 , 568.4 , and 657.1 cm^{-1} correspond to Ni–O, $\text{Co}^{2+}\text{--O}$ and $\text{Co}^{3+}\text{--O}$ respectively. The characteristic peaks at 3440 cm^{-1} (O–H stretching

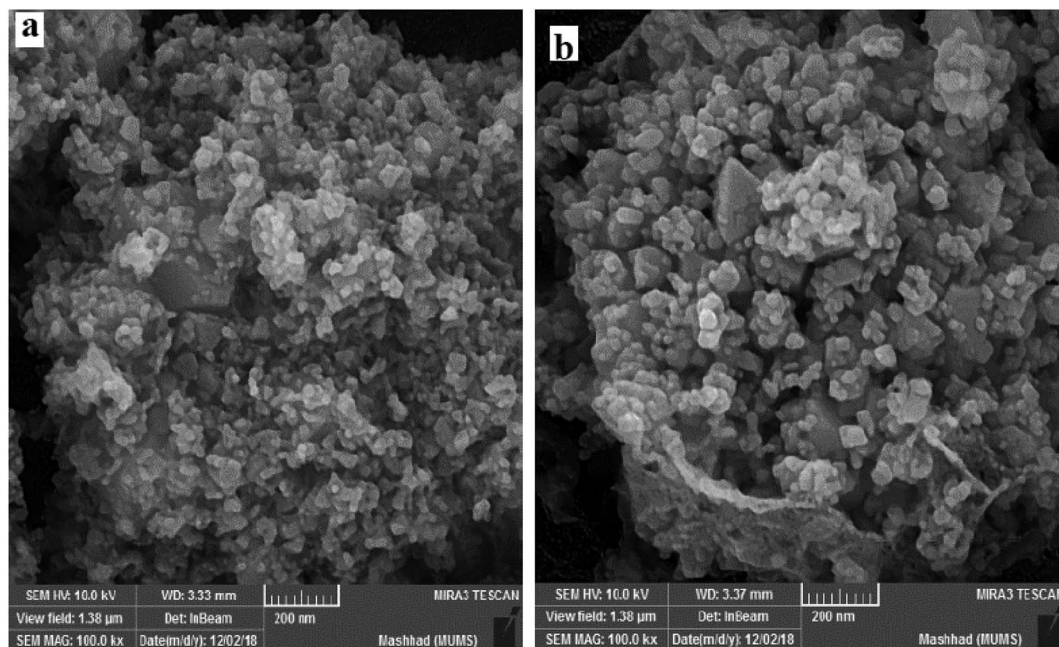


Fig. 2 SEM images of (a) $\text{Co}_3\text{O}_4/\text{NiO}$ and (b) $\text{Co}_3\text{O}_4/\text{NiO}@GQD@SO_3\text{H}$.



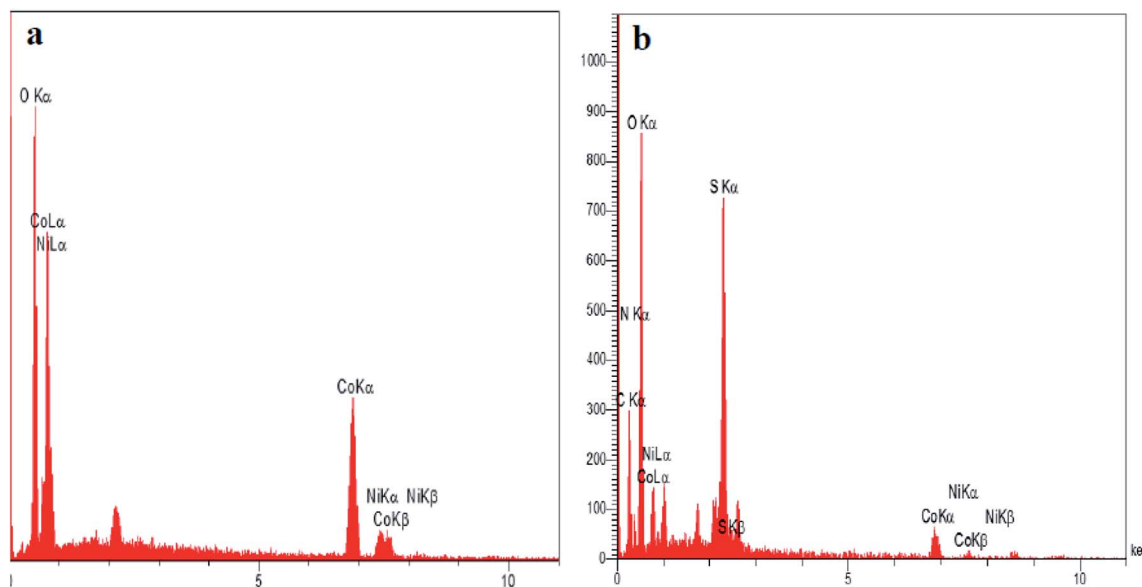


Fig. 3 EDS spectra of (a) $\text{Co}_3\text{O}_4/\text{NiO}$ and (b) $\text{Co}_3\text{O}_4/\text{NiO}@GQD@SO_3H$.

vibration), 1705 cm^{-1} ($\text{C}=\text{O}$ stretching vibration), and 1125 cm^{-1} ($\text{C}-\text{O}-\text{C}$ stretching vibration) appear in the spectrum in Fig. 5b. The peak at approximately $1475\text{--}1580\text{ cm}^{-1}$ is attributed to the $\text{C}=\text{C}$ bonds. The presence of the sulfonyl group is also verified by the peaks at 1215 and 1120 cm^{-1} . The broad peak at 3350 cm^{-1} is related to the stretching vibrational absorptions of OH (SO_3H) (Fig. 5c).

The BET specific surface area of the $\text{Co}_3\text{O}_4/\text{NiO}$ and $\text{Co}_3\text{O}_4/\text{NiO}@GQD@SO_3H$ nanocomposites was measured by nitrogen gas adsorption-desorption isotherms (Fig. 6). The results

indicate that the BET specific surface area of $\text{Co}_3\text{O}_4/\text{NiO}$ improved from 12.25 to $32.43\text{ m}^2\text{ g}^{-1}$ after modification with the GQDs; therefore, more active sites were introduced on the surface of $\text{Co}_3\text{O}_4/\text{NiO}@GQD@SO_3H$.

TGA (thermogravimetric analysis) was used to evaluate the thermal stability of the $\text{Co}_3\text{O}_4/\text{NiO}@GQD@SO_3H$ nanocomposite. The nanocomposite displayed suitable thermal stability without a significant decrease in weight (Fig. 7). The weight loss at temperatures below $210\text{ }^\circ\text{C}$ is owing to the removal of physically adsorbed solvent and surface hydroxyl

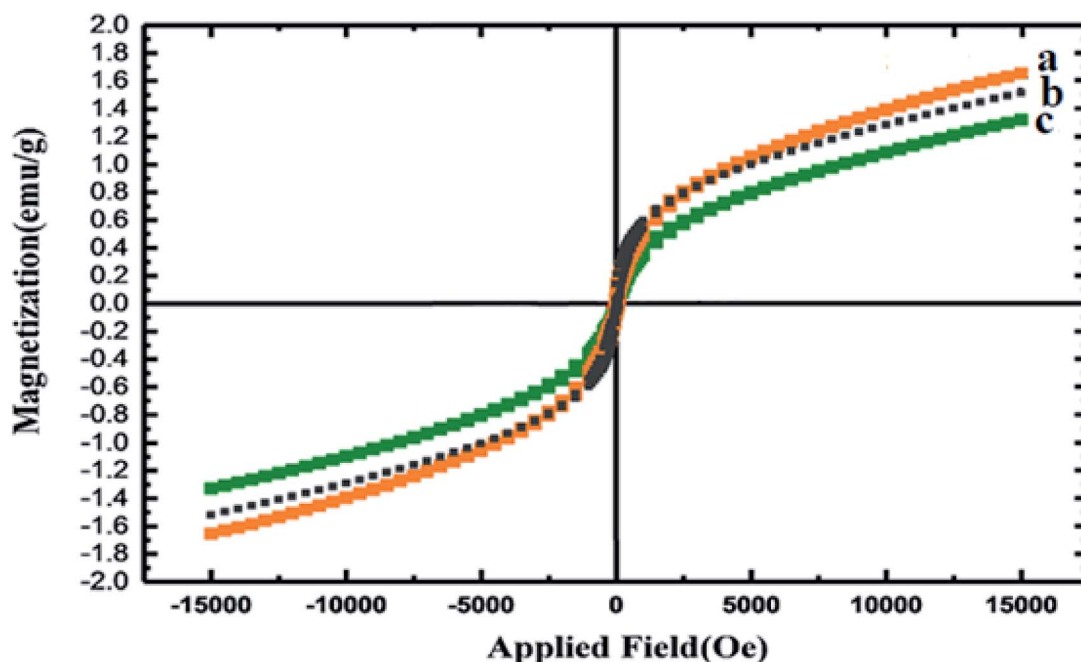


Fig. 4 VSM curves of (a) $\text{Co}_3\text{O}_4/\text{NiO}$, (b) $\text{Co}_3\text{O}_4/\text{NiO}@GQDs$ and (c) $\text{Co}_3\text{O}_4/\text{NiO}@GQD@SO_3H$.



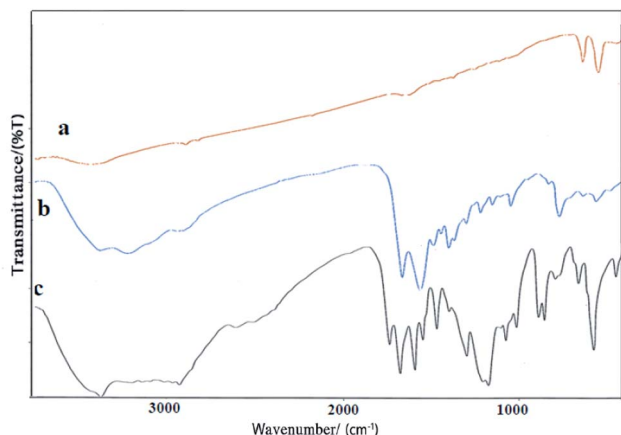


Fig. 5 FT-IR spectra of (a) $\text{Co}_3\text{O}_4/\text{NiO}$, (b) $\text{Co}_3\text{O}_4/\text{NiO@GQDs}$ and (c) $\text{Co}_3\text{O}_4/\text{NiO@GQD@SO}_3\text{H}$.

groups. The curve indicates a weight loss of about 14.06% from 150 °C to 500 °C, which is attributed to the oxidation and degradation of the GQD.

The X-ray photoelectron spectroscopy (XPS) analysis of the $\text{Co}_3\text{O}_4/\text{NiO@GQD@SO}_3\text{H}$ nanocomposite is shown in Fig. 8. In the wide-scan spectrum of the nanocatalyst, the predominant components are Ni 2p_{1/2} (873.4 eV), Ni 2p_{3/2} (854.4 eV), Co 2p_{1/2} (792.6 eV), Co 2p_{3/2} (780.4 eV), O 1s (529.8 eV), N 1s (400 eV), C 1s (284.5 eV) and S 2p (164.3 eV).

Initially, we carried out a three-component reaction with 4-nitrobenzaldehyde, 6-amino-1,3-dimethyluracil and 4-hydroxycoumarin as a model reaction. The model reactions were performed in the presence of NaHSO_4 , ZrO_2 , *p*-TSA, Co_3O_4 , NiO, $\text{Co}_3\text{O}_4/\text{NiO}$, $\text{Co}_3\text{O}_4/\text{NiO@GQDs}$ and $\text{Co}_3\text{O}_4/\text{NiO@GQD@SO}_3\text{H}$ nanocomposite as catalysts. The reactions were tested using diverse solvents including ethanol, acetonitrile, water and dimethylformamide. The best results were obtained in EtOH and we found that the reaction gave convincing results in the presence of the $\text{Co}_3\text{O}_4/\text{NiO@GQD@SO}_3\text{H}$ nanocomposite (5 mg) under reflux conditions (Table 1).

A series of aromatic aldehydes were studied under the optimum conditions (Table 2). Good yields were obtained using

aromatic aldehydes either bearing electron-withdrawing substituents or electron-donating substituents.

We also investigated the recyclability of the $\text{Co}_3\text{O}_4/\text{NiO@GQD@SO}_3\text{H}$ nanocomposite as a catalyst for the model reaction under reflux conditions in ethanol. The results showed that nanocomposite can be reused several times without noticeable loss in its catalytic activity (yield in the range of 93% to 91%) (Fig. 9).

The plausible mechanism for the preparation of chromenpyrimidines using the $\text{Co}_3\text{O}_4/\text{NiO@GQD@SO}_3\text{H}$ nanocomposite is shown in Scheme 2. Firstly, we assumed that the reaction occurs *via* condensation between 6-amino-1,3-dimethyluracil and aldehyde to form intermediate **I** on the active sites of the $\text{Co}_3\text{O}_4/\text{NiO@GQD@SO}_3\text{H}$ nanocatalyst. Then, 4-hydroxycoumarin is added to intermediate **I** to give intermediate **II**. Then, migration of the hydrogen atom provides the final product (Scheme 2).

To study the applicability of this method for large-scale synthesis, we performed selected reactions at the 10 mmol scale. As can be seen, the reactions on a large scale gave the product with a gradual decrease in reaction yield (Table 3).

To compare the efficiency of the $\text{Co}_3\text{O}_4/\text{NiO@GQD@SO}_3\text{H}$ nanocomposite with the reported catalysts for the synthesis of chromenpyrimidines, we tabulated the results in Table 4. As indicated in Table 4, the $\text{Co}_3\text{O}_4/\text{NiO@GQD@SO}_3\text{H}$ nanocomposite is superior to the reported catalysts. As expected, the increased surface area due to the small particle size increased the reactivity of the catalyst, which is responsible for the accessibility of the substrate molecules on the catalyst surface.

The activity of catalysts is influenced by their acid-base properties and many other factors such as surface area, geometric structure (particularly pore structure), distribution of sites and polarity of the surface sites.^{41,42} The SO_3H groups distributed on the surface of $\text{Co}_3\text{O}_4/\text{NiO@GQDs}$ activate the groups of the substrates. In this mechanism, the surface atoms of $\text{Co}_3\text{O}_4/\text{NiO@GQD@SO}_3\text{H}$ activate the C=O and C=N groups for better reaction with nucleophiles. The $\text{Co}_3\text{O}_4/\text{NiO@GQD@SO}_3\text{H}$ nanocomposite has Lewis and Brønsted acid properties, which increase the activity of the catalyst.

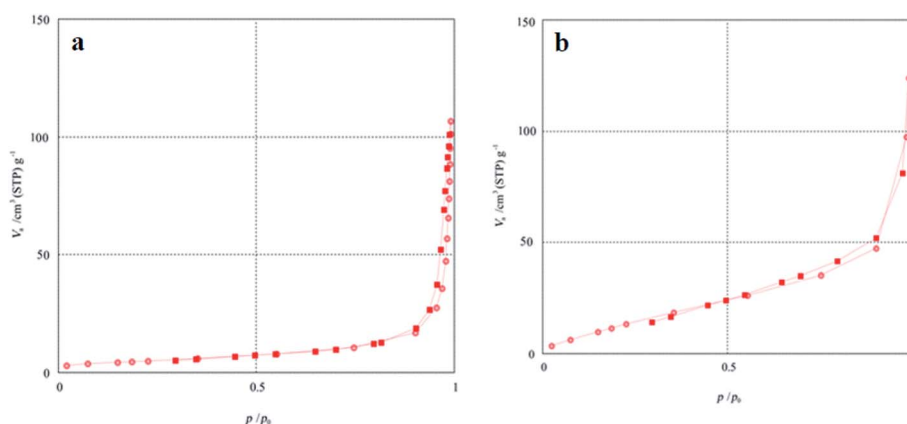


Fig. 6 BET specific surface area of (a) $\text{Co}_3\text{O}_4/\text{NiO}$ and (b) $\text{Co}_3\text{O}_4/\text{NiO@GQD@SO}_3\text{H}$.



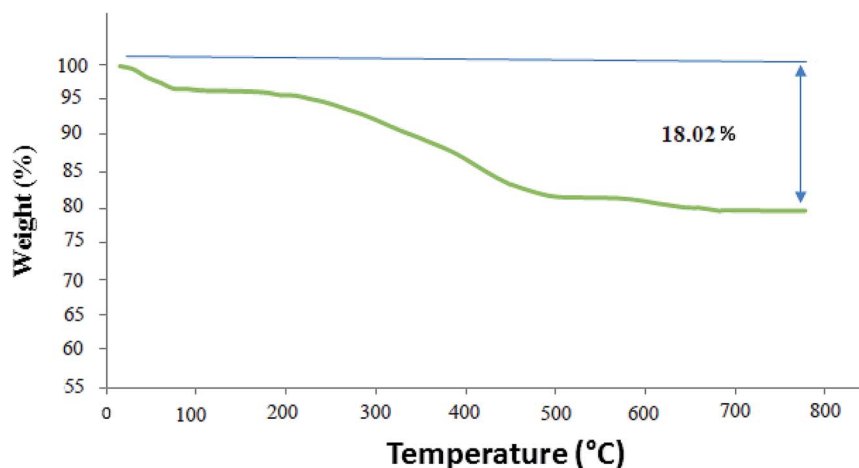


Fig. 7 TGA of $\text{Co}_3\text{O}_4/\text{NiO}@\text{GQD}@\text{SO}_3\text{H}$ nanocomposite.

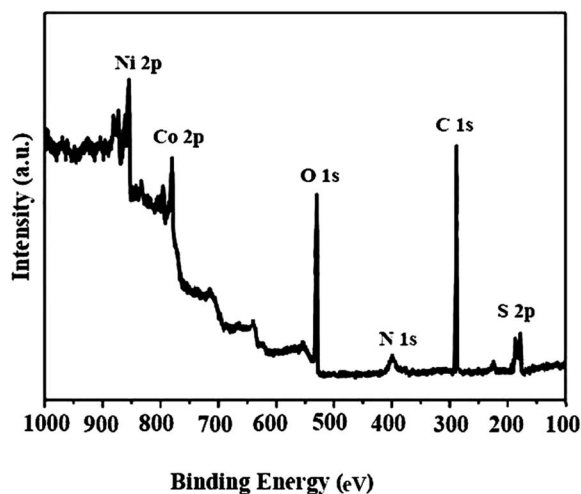


Fig. 8 X-ray photoelectron spectroscopy (XPS) analysis of the $\text{Co}_3\text{O}_4/\text{NiO}@\text{GQD}@\text{SO}_3\text{H}$ nanocomposite.

3. Experimental

3.1. Chemicals and apparatus

NMR spectra were recorded on a Bruker Avance-400 MHz spectrometer in the presence of tetramethylsilane as an internal standard. IR spectra were recorded on an FT-IR Magna 550 spectrometer using KBr plates. Melting points were determined on an Electrothermal 9200, and are not corrected. Elemental analyses (C, H, and N) were performed on a Carlo ERBA Model EA 1108 analyzer. Powder X-ray diffraction (XRD) was performed on a Philips X'pert diffractometer with monochromatized $\text{Cu K}\alpha$ radiation ($\lambda = 1.5406 \text{ \AA}$). The microscopic morphology of the nanocatalyst was visualized by SEM (MIRA3). Thermogravimetric analysis (TGA) curves were measured on a V5.1A DUPONT 2000. The magnetic measurement of the samples was performed in a vibrating sample magnetometer (VSM) (Meghnatis Daghigh Kavir Co.; Kashan Kavir; Iran).

3.2. Preparation of $\text{Co}_3\text{O}_4/\text{NiO}$ nanoparticles

$\text{Co}(\text{NO}_3)_3$ and NiCl_2 with a 3 : 1 molar ratio were dissolved in ethylene glycol. Afterward, the appropriate amount of aqueous ammonia solution (28 wt%) was added to the above solution until the pH reached 10. Then, the transparent solution was placed in an autoclave at 150°C for 4 h. The obtained precipitate was washed twice with methanol and dried at 60°C for 8 h. Finally, the product was calcined at 500°C for 2 h.

3.3. Preparation of $\text{Co}_3\text{O}_4/\text{NiO}@\text{N-GQD}$ nanocomposite

1 g citric acid was dissolved in 20 mL deionized water, and stirred to form a clear solution. Subsequently, 0.3 mL ethylenediamine was added to the above solution and mixed to obtain a clear solution. Then, 0.1 g $\text{Co}_3\text{O}_4/\text{NiO}$ nanoparticles were added to the mixture. The mixture was stirred at room temperature for 5 min. Then the solution was transferred to a 50 mL Teflon-lined stainless autoclave, which was sealed and heated to 180°C for 12 h in an electric oven. Finally, the as-prepared nanostructured $\text{Co}_3\text{O}_4/\text{NiO}@\text{GQDs}$ was obtained, which was washed several times with deionized water and ethanol, and then dried in an oven until a constant weight was achieved.

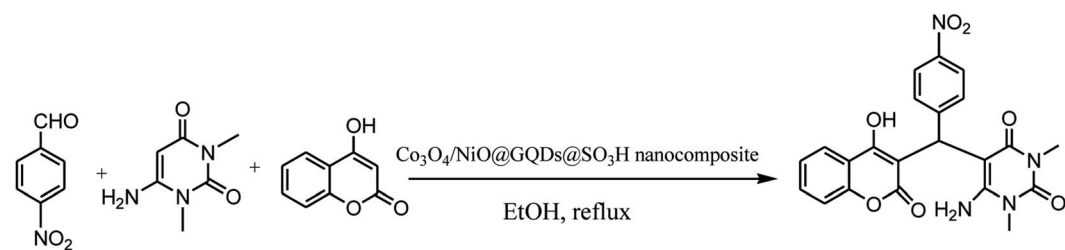
3.4. Preparation of $\text{Co}_3\text{O}_4/\text{NiO}@\text{GQD}@\text{SO}_3\text{H}$ nanocomposite

1 g of $\text{Co}_3\text{O}_4/\text{NiO}@\text{N-GQD}$ nanocomposite was dispersed in dry CH_2Cl_2 (10 mL) and sonicated for 5 min. Then, chlorosulfonic acid (0.8 mL in dry CH_2Cl_2) was added dropwise to a cooled (ice-bath) mixture of $\text{Co}_3\text{O}_4/\text{NiO}@\text{N-GQDs}$ for 30 min under N_2 with vigorous stirring. The mixture was stirred for 120 min, while the residual HCl was removed by suction. The resulted $\text{Co}_3\text{O}_4/\text{NiO}@\text{GQD}@\text{SO}_3\text{H}$ nanocomposite was separated, washed several times with dried CH_2Cl_2 before drying under vacuum at 60°C .

3.5. General procedure for the preparation of chromenpyrimidines

A mixture of aldehyde (1 mmol), 6-amino-1,3-dimethyluracil (1 mmol), 4-hydroxycoumarin (1 mmol) and 5 mg $\text{Co}_3\text{O}_4/$



Table 1 Optimization of the reaction conditions using different catalysts^a


Entry	Catalyst (amount)	Solvent (reflux)	Time (min)	Conversion efficiency	Yield ^b (%)
1	None	EtOH	300	NR	NR
2	Et ₃ N (5 mol%)	EtOH	300	28	35
3	NaHSO ₄ (4 mol%)	EtOH	250	37	42
4	ZrO ₂ (4 mol%)	EtOH	250	43	48
5	<i>p</i> TSA NPs (5 mol%)	EtOH	250	49	54
6	Nano-Co ₃ O ₄	EtOH	250	40	45
7	Nano-NiO	EtOH	250	45	52
8	Co ₃ O ₄ /NiO nanocomposite	EtOH	250	55	60
9	Co ₃ O ₄ /NiO@GQD nanocomposite	EtOH	150	68	72
10	Co ₃ O ₄ /NiO@GQD@SO ₃ H nanocomposite (3 mg)	EtOH	80	81	85
11	Co ₃ O ₄ /NiO@GQD@SO ₃ H nanocomposite (5 mg)	EtOH	80	87	93
12	Co ₃ O ₄ /NiO@GQD@SO ₃ H nanocomposite (7 mg)	EtOH	80	87	93
13	Co ₃ O ₄ /NiO@GQD@SO ₃ H nanocomposite (5 mg)	H ₂ O	100	69	72
14	Co ₃ O ₄ /NiO@GQD@SO ₃ H nanocomposite (5 mg)	DMF	90	71	76
15	Co ₃ O ₄ /NiO@GQD@SO ₃ H nanocomposite (5 mg)	CH ₃ CN	80	77	82

^a 4-Nitrobenzaldehyde (1 mmol), 6-amino-1,3-dimethyluracil (1 mmol) and 4-hydroxycoumarin (1 mmol). ^b Isolated yield.

NiO@GQD@SO₃H nanocomposite was stirred in 5 mL ethanol under reflux. The reaction was monitored by TLC. After completion of the reaction, the solution was filtered, and the heterogeneous catalyst was recovered. Water was added, and the precipitate was collected by filtration and washed with water. The crude product was recrystallized or washed with ethanol to give the pure product.

3.6. Spectral data

6-Amino-5-((4-hydroxy-2-oxo-2H-chromen-3-yl)(phenyl)methyl)-1,3-dimethylpyrimidine-2,4(1H,3H)-dione (4a). White solid; m.p. 220–222 °C; IR (KBr): 3432, 3234, 2964, 1695, 1664, 1616, 1569, 1444, 1356, 754 cm⁻¹; ¹H NMR (400 MHz, DMSO-*d*₆) δ: 3.14 (s, 3H, -CH₃), 3.40 (s, 3H, -CH₃), 5.62 (s, 1H, -CH), 7.16–7.85 (m, 11H, ArH, -NH₂), 13.99 (s, 1H, -OH); ¹³C NMR (100 MHz, DMSO-*d*₆) δ: 28.68, 31.02, 36.53, 87.26, 105.11, 116.62, 117.41, 124.17, 124.76, 126.14, 126.80, 128.55, 132.87, 138.74, 150.50, 152.44, 155.63, 164.27, 164.55, 166.27; anal. calcd for C₂₂H₁₉N₃O₅: C, 65.18%; H, 4.72%; N, 10.37%. Found: C, 65.20%; H, 4.59%; N, 10.25%.

6-Amino-5-((4-hydroxy-2-oxo-2H-chromen-3-yl)(4-chlorophenyl)methyl)-1,3-dimethylpyrimidine-2,4(1H,3H)-dione (4b). White solid; m.p. 218–220 °C; IR (KBr): 3405, 3211, 2921, 1695, 1663, 1617, 1493, 1448, 763 cm⁻¹; ¹H NMR (400 MHz, DMSO-*d*₆) δ: 3.14 (s, 3H), 3.37 (s, 3H), 5.61 (s, 1H), 7.17–7.85 (m, 10H, ArH and NH₂), 13.98 (s, 1H, OH); ¹³C NMR (100 MHz, DMSO-*d*₆) δ: 28.72, 31.14, 36.17, 86.98, 104.96, 116.60,

117.35, 124.20, 124.82, 128.43, 128.96, 130.78, 132.96, 138.02, 150.52, 152.40, 155.62, 164.25, 164.52, 166.14; anal. calcd for C₂₂H₁₈ClN₃O₅: C, 60.07%; H, 4.12%; N, 9.55%. Found: C, 60.15%; H, 4.18%; N, 9.42%.

6-Amino-5-((4-hydroxy-2-oxo-2H-chromen-3-yl)(4-methoxyphenyl)methyl)-1,3-dimethylpyrimidine-2,4(1H,3H)-dione (4c). Light yellow solid, m.p.: 178–180 °C; IR (KBr): 3413, 3238, 2952, 1695, 1613, 1568, 1508, 1450, 1253, 767 cm⁻¹; ¹H NMR (400 MHz, DMSO-*d*₆) δ: 3.14 (s, 3H), 3.37 (s, 3H), 3.69 (s, 3H), 5.61 (s, 1H), 6.78–6.80 (d, *J* = 8.0 Hz, 2H), 7.03–7.05 (d, *J* = 8.0 Hz, 2H), 7.32–7.84 (m, 6H), 13.98 (s, 1H, OH); ¹³C NMR (100 MHz, DMSO-*d*₆) δ: 28.66, 31.02, 35.83, 55.43, 87.45, 105.43, 113.95, 116.62, 117.42, 124.15, 124.75, 127.90, 130.32, 132.82, 150.56, 152.42, 155.57, 157.88, 164.20, 164.54, 166.29; anal. calcd for C₂₃H₂₁N₃O₆: C, 63.44%; H, 4.86%; N, 9.65%. Found: C, 63.49%; H, 4.74%; N, 9.59%.

6-Amino-5-((4-hydroxy-2-oxo-2H-chromen-3-yl)(4-nitrophenyl)methyl)-1,3-dimethylpyrimidine-2,4(1H,3H)-dione (4d). Light yellow solid; m.p.: 240–242 °C; IR (KBr): 3396, 3210, 2903, 1685, 1619, 1571, 1514, 1346, 769 cm⁻¹; ¹H NMR (400 MHz, DMSO-*d*₆) δ: 3.14 (s, 3H), 3.49 (s, 3H), 5.75 (s, 1H), 7.35–8.10 (m, 10H), 13.96 (s, 1H, OH); ¹³C NMR (100 MHz, DMSO-*d*₆) δ: 28.69, 31.05, 36.52, 86.48, 104.72, 117.30, 121.45, 121.63, 124.22, 130.00, 133.04, 134.12, 141.74, 148.41, 150.46, 152.47, 155.80, 164.34, 164.55, 165.98; anal. calcd for C₂₂H₁₈N₄O₇: C, 58.67%; H, 4.03%; N, 12.44%; found C, 58.72%; H, 4.09%; N, 12.52%.



Table 2 Synthesis of chromenpyrimidines using the Co₃O₄/NiO@GQD@SO₃H nanocomposite (5 mg) under reflux conditions^a

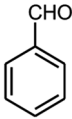
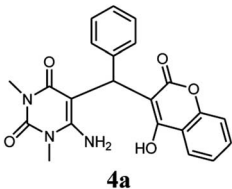

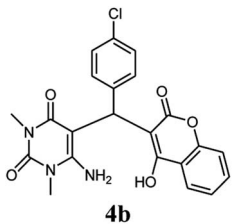
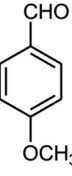
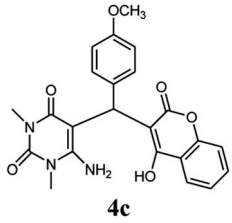
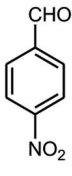
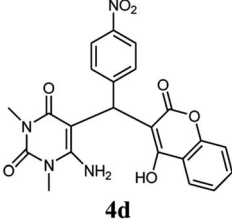
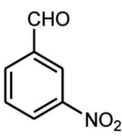
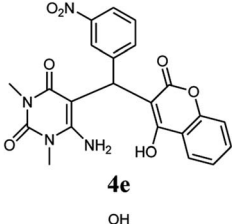
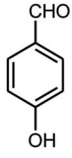
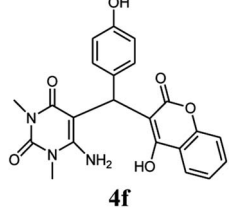
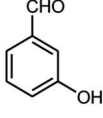
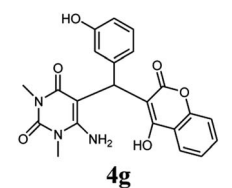
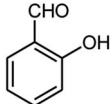
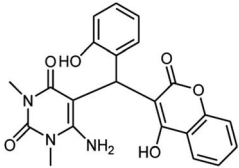
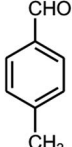
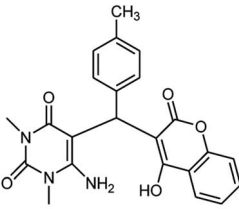
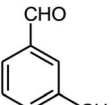
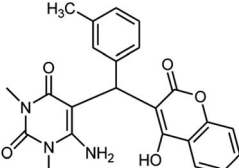
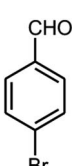
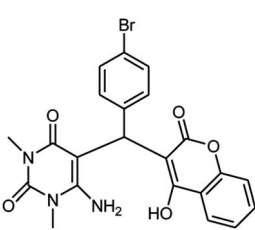
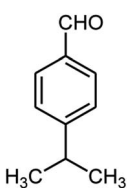
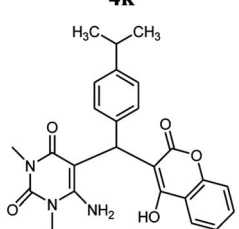
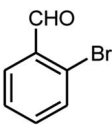
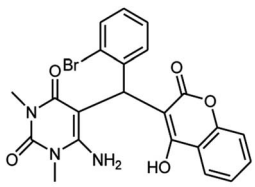
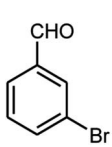
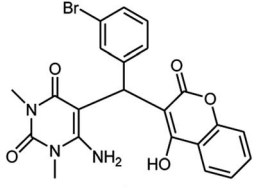
Entry	Aldehyde (1a–1l)	Product	Time (min)	Conversion efficiency	Yield ^b (%)	mp (°C) (ref.)	mp (°C) (reported)
1		 4a	80	80	88	218–220 (10)	220–222
2		 4b	80	82	90	219–220 (10)	218–220
3		 4c	90	72	85	180–181 (10)	178–180
4		 4d	80	87	93	240–242 (13)	240–242
5		 4e	80	80	88	230–232 (10)	230–232
6		 4f	110	75	83	—	230–232
7		 4g	100	77	87	—	232–234



Table 2 (Contd.)

Entry	Aldehyde (1a–1l)	Product	Time (min)	Conversion efficiency	Yield ^b (%)	mp (°C) (ref.)	mp (°C) (reported)
8		 4h	110	74	81	—	240–242
9		 4i	90	76	85	202–204 (10)	202–204
10		 4j	85	80	87	—	200–202
11		 4k	80	81	89	236–238 (10)	236–238
12		 4l	100	74	84	257–259 (13)	257–259
13		 4m	80	79	89	210–212 (10)	210–212
14		 4n	80	81	88	245–247 (13)	245–247

^a Aromatic aldehydes (1 mmol), 6-amino-1,3-dimethyluracil (1 mmol) and 4-hydroxycoumarin (1 mmol). ^b Isolated yield.



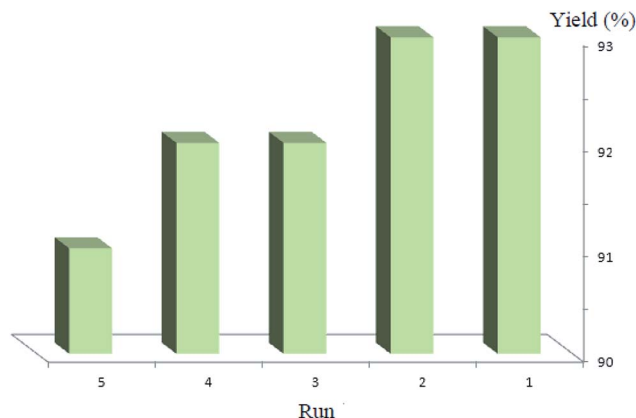


Fig. 9 Recycling of the $\text{Co}_3\text{O}_4/\text{NiO}@\text{GQD}@\text{SO}_3\text{H}$ nanocomposite as a catalyst for the model reaction.

6-Amino-5-((4-hydroxy-2-oxo-2H-chromen-3-yl)(3-nitrophenyl) methyl)-1,3-dimethylpyrimidine-2,4(1H,3H)-dione (4e). Light yellow solid; m.p.: 230–232 °C; IR (KBr): 3460, 3209, 2923, 1699, 1673, 1523, 1437, 1343, 772 cm^{-1} ; ^1H NMR (400 MHz, $\text{DMSO}-d_6$) δ : 3.14 (s, 3H), 3.38 (s, 3H), 5.76 (s, 1H), 7.36–8.06 (m, 10H), 13.97 (s, 1H, OH); ^{13}C NMR (100 MHz, $\text{DMSO}-d_6$) δ : 28.69, 31.05, 36.52, 86.48, 104.70, 116.54, 117.35, 121.42, 121.62, 124.80, 124.24, 130.14, 133.24, 134.22, 141.75, 148.45, 150.49, 152.42, 155.92, 164.42, 164.45, 165.85; anal. calcd for $\text{C}_{22}\text{H}_{18}\text{N}_4\text{O}_7$: C, 58.67%; H, 4.03%; N, 12.44%; found C, 58.75%; H, 4.12%; N, 12.54%.

6-Amino-5-((4-hydroxy-2-oxo-2H-chromen-3-yl)(4-hydroxyphenyl) methyl)-1,3-dimethylpyrimidine-2,4(1H,3H)-dione (4f). White solid; m.p. 230–232 °C; IR (KBr): 3364, 3219, 1695, 1671, 1569, 1509, 1444, 1358, 769 cm^{-1} ; ^1H NMR (400 MHz, $\text{DMSO}-d_6$) δ : 3.14 (s, 3H), 3.49 (s, 3H), 5.51 (s, 1H), 6.60–6.62 (d, J = 8.0 Hz, 2H), 6.90–6.92 (d, J = 8.0 Hz, 2H), 7.29–7.84

Table 3 The large-scale synthesis of some chromenpyrimidines using the $\text{Co}_3\text{O}_4/\text{NiO}@\text{GQD}@\text{SO}_3\text{H}$ nanocomposite (5 mg)

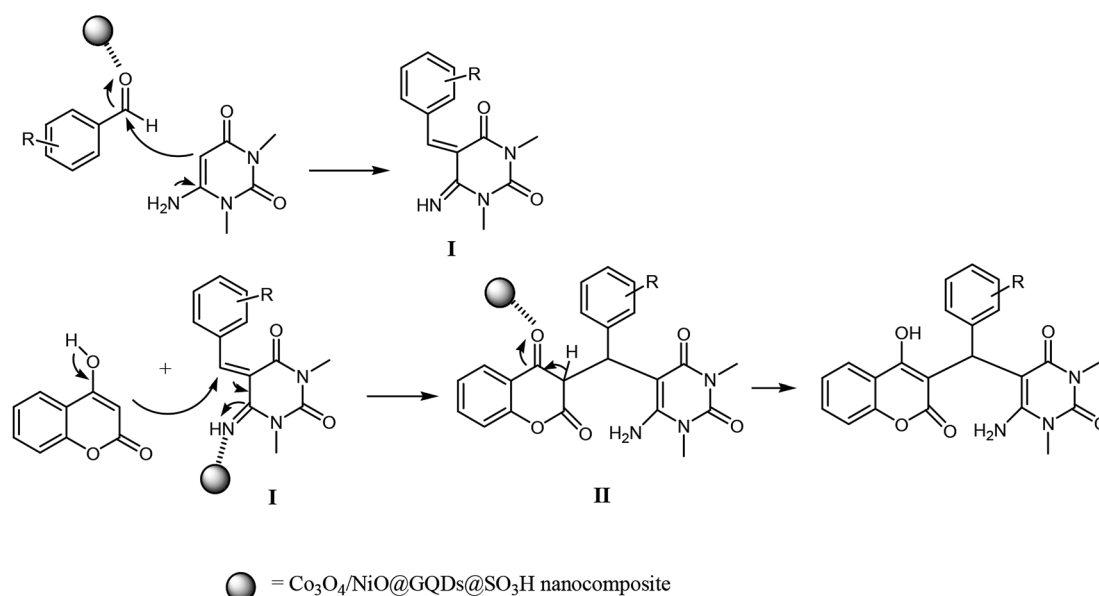
Entry	Product	Time (min)	Yield ^a (%)
1	4a	90	86
2	4c	95	83
3	4d	80	90
4	4i	95	82
5	4k	80	87

^a Isolated yield.

(m, 6H), 9.14 (s, 1H, OH), 13.97 (s, 1H, OH); ^{13}C NMR (100 MHz, $\text{DMSO}-d_6$) δ : 28.64, 30.96, 35.74, 87.54, 105.45, 115.35, 116.55, 117.40, 124.12, 124.73, 127.77, 128.41, 132.79, 150.50, 152.35, 155.43, 155.76, 164.17, 164.49, 166.27. Anal. calcd for $\text{C}_{22}\text{H}_{19}\text{N}_3\text{O}_6$: C, 62.70%; H, 4.54%; N, 9.97%; found C, 62.78%; H, 4.59%; N, 10.05%.

6-Amino-5-((4-hydroxy-2-oxo-2H-chromen-3-yl)(3-hydroxyphenyl) methyl)-1,3-dimethylpyrimidine-2,4(1H,3H)-dione (4g). White solid; m.p. 232–234 °C; IR (KBr): 3429, 3306, 2957, 1695, 1670, 1617, 1569, 1447, 1354, 760 cm^{-1} ; ^1H NMR (400 MHz, $\text{DMSO}-d_6$) δ : 3.15 (s, 3H), 3.38 (s, 3H), 5.55 (s, 1H), 6.53–7.67 (m, 10H), 9.12 (s, 1H, OH), 14.03 (s, 1H, OH); ^{13}C NMR (100 MHz, $\text{DMSO}-d_6$) δ : 28.72, 30.94, 35.72, 87.55, 104.55, 115.34, 116.52, 116.58, 117.42, 124.14, 124.25, 124.78, 127.75, 128.43, 132.79, 151.22, 152.34, 155.42, 155.78, 164.15, 164.45, 166.28. Anal. calcd for $\text{C}_{22}\text{H}_{19}\text{N}_3\text{O}_6$: C, 62.70%; H, 4.54%; N, 9.97%; found C, 62.72%; H, 4.55%; N, 10.09%.

6-Amino-5-((4-hydroxy-2-oxo-2H-chromen-3-yl)(2-hydroxyphenyl) methyl)-1,3-dimethylpyrimidine-2,4(1H,3H)-dione (4h). White solid; m.p. 240–242 °C; IR (KBr): 3432, 3306, 2958, 1695, 1607, 1617, 1447, 760 cm^{-1} ; ^1H NMR (400 MHz, $\text{DMSO}-d_6$) δ : 3.15 (s, 3H), 3.38 (s, 3H), 5.55 (s, 1H), 6.63–7.87 (m,



Scheme 2 Proposed mechanism for the three-component reaction.



Table 4 Comparison of the catalytic activity of the $\text{Co}_3\text{O}_4/\text{NiO}@G\text{QD}@SO_3\text{H}$ nanocomposite (5 mg) with that of other reported catalysts for the synthesis chromenpyrimidines (**4b**)

Entry	Catalyst (conditions)	Time (min)	Conversion efficiency	Yield ^a (%)	Ref.
1	L-proline, 20 mol%, EtOH, reflux	360	75	83	13
2	Bifunctional thiourea-based organocatalyst, 20 mol%, H_2O , reflux	240	79	86	14
3	Sulfamic acid, 30 mol%, ($\text{EtOH} : \text{H}_2\text{O} : 1 : 1$), ultrasound irradiation	30	77	85	11
4	$\text{Co}_3\text{O}_4/\text{NiO}@G\text{QD}@SO_3\text{H}$ nanocomposite (5 mg, EtOH, reflux)	80	82	90	This work

^a Isolated yield.

10H), 9.11 (s, 1H, OH), 14.03 (s, 1H, OH); ^{13}C NMR (100 MHz, $\text{DMSO}-d_6$) δ : 28.67, 31.02, 36.40, 87.35, 104.98, 113.16, 113.69, 116.58, 116.59, 117.48, 124.23, 124.81, 124.83, 129.47, 132.93, 140.27, 150.51, 152.36, 155.52, 157.72, 164.48, 166.23. Anal. calcd for $\text{C}_{22}\text{H}_{19}\text{N}_3\text{O}_6$: C, 62.70%; H, 4.54%; N, 9.97%; found C, 62.82%; H, 4.62%; N, 9.98%.

6-Amino-5-((4-hydroxy-2-oxo-2H-chromen-3-yl)(4-methylphenyl) methyl)-1,3-dimethylpyrimidine-2,4(1H,3H)-dione (4i). White solid; m.p. 202–204 °C; IR (KBr): 3411, 3212, 2922, 1697, 1665, 1618, 1569, 1353, 764 cm^{-1} ; ^1H NMR (400 MHz, $\text{DMSO}-d_6$) δ : 2.24 (s, 3H), 3.14 (s, 3H), 3.37 (s, 3H), 5.57 (s, 1H), 6.96–7.85 (m, 10H), 13.98 (s, 1H, OH); ^{13}C NMR (100 MHz, $\text{DMSO}-d_6$) δ : 20.60, 28.32, 30.64, 35.74, 87.30, 104.72, 116.25, 123.72, 124.17, 124.42, 126.37, 128.82, 132.58, 134.74, 135.13, 150.18, 152.02, 155.12, 164.15, 165.93, 167.75; anal. calcd for $\text{C}_{23}\text{H}_{21}\text{N}_3\text{O}_5$: C, 65.86%; H, 5.05%; N, 10.02%; found C, 65.92%; H, 5.15%; N, 10.08%.

6-Amino-5-((4-hydroxy-2-oxo-2H-chromen-3-yl)(3-methylphenyl) methyl)-1,3-dimethylpyrimidine-2,4(1H,3H)-dione (4j). White solid; m.p. 200–202 °C; IR (KBr): 3403, 3229, 2923, 1699, 1695, 1445, 758 cm^{-1} ; ^1H NMR (400 MHz, $\text{DMSO}-d_6$) δ : 2.21 (s, 3H), 3.15 (s, 3H), 3.38 (s, 3H), 5.59 (s, 1H), 6.92–7.86 (m, 10H), 13.97 (s, 1H, OH); ^{13}C NMR (100 MHz, $\text{DMSO}-d_6$) δ : 21.63, 28.66, 30.98, 36.37, 87.34, 105.11, 116.58, 117.37, 123.91, 124.18, 124.77, 126.87, 127.29, 128.42, 132.85, 137.50, 138.66, 150.50, 152.37, 155.52, 164.26, 164.54, 166.25; anal. calcd for $\text{C}_{23}\text{H}_{21}\text{N}_3\text{O}_5$: C, 65.86%; H, 5.05%; N, 10.02%; found C, 65.96%; H, 5.18%; N, 10.12%.

6-Amino-5-((4-hydroxy-2-oxo-2H-chromen-3-yl)(4-bromophenyl) methyl)-1,3-dimethylpyrimidine-2,4(1H,3H)-dione (4k). White solid; m.p. 236–238 °C; IR (KBr): 3404, 3212, 2921, 1675, 1663, 1616, 1488, 1446, 761 cm^{-1} ; ^1H NMR (400 MHz, $\text{DMSO}-d_6$) δ : 3.13 (s, 3H), 3.37 (s, 3H), 5.58 (s, 1H), 7.11–7.84 (m, 10H), 13.97 (s, 1H, OH); ^{13}C NMR (100 MHz, $\text{DMSO}-d_6$) δ : 28.75, 31.17, 36.19, 86.95, 104.93, 116.63, 117.34, 124.22, 124.85, 128.40, 128.93, 130.79, 132.94, 138.08, 150.55, 152.42, 155.67, 164.28, 164.54, 166.16; anal. calcd for $\text{C}_{22}\text{H}_{18}\text{BrN}_3\text{O}_5$: C, 54.56%; H, 3.75%; N, 8.68%. Found: C, 54.62%; H, 3.83%; N, 8.75%.

6-Amino-5-((4-hydroxy-2-oxo-2H-chromen-3-yl)(4-isopropylphenyl) methyl)-1,3-dimethylpyrimidine-2,4(1H,3H)-dione (4l). White solid; m.p. 257–259 °C; IR (KBr): 3463, 3230, 2958, 1695, 1671, 1616, 1569, 1446, 1343, 762 cm^{-1} ; ^1H NMR (400 MHz, $\text{DMSO}-d_6$) δ : 1.15 (s, 6H), 2.77 (m, 1H), 3.15

(s, 3H), 3.38 (s, 3H), 5.57 (s, 1H), 7.02–7.85 (m, 10H), 13.99 (s, 1H, OH); ^{13}C NMR (100 MHz, $\text{DMSO}-d_6$) δ : 23.8, 28.1, 30.3, 32.9, 35.6, 87.1, 104.4, 115.8, 116.9, 123.7, 123.9, 125.8, 126.1, 131.9, 135.2, 145.5, 149.9, 151.9, 155.0, 163.8, 164.1, 168.3; anal. calcd for $\text{C}_{25}\text{H}_{25}\text{N}_3\text{O}_5$: C, 67.10%; H, 5.63%; N, 9.39%; found C, 67.19%; H, 5.75%; N, 9.45%.

6-Amino-5-((4-hydroxy-2-oxo-2H-chromen-3-yl)(2-bromophenyl) methyl)-1,3-dimethylpyrimidine-2,4(1H,3H)-dione (4m). White solid; m.p. 210–212 °C; IR (KBr): 3402, 3210, 2925, 1676, 1665, 1618, 1489, 1447, 765 cm^{-1} ; ^1H NMR (400 MHz, $\text{DMSO}-d_6$) δ : 3.12 (s, 3H), 3.35 (s, 3H), 5.57 (s, 1H), 7.12–7.86 (m, 10H), 13.96 (s, 1H, OH); ^{13}C NMR (100 MHz, $\text{DMSO}-d_6$) δ : 28.74, 31.16, 36.10, 86.94, 104.92, 116.63, 117.29, 124.25, 124.82, 126.35, 127.52, 128.40, 128.92, 130.75, 132.96, 138.05, 150.56, 152.47, 155.65, 164.22, 164.55, 166.14; anal. calcd for $\text{C}_{22}\text{H}_{18}\text{BrN}_3\text{O}_5$: C, 54.56%; H, 3.75%; N, 8.68%. Found: C, 54.65%; H, 3.86%; N, 8.77%.

6-Amino-5-((4-hydroxy-2-oxo-2H-chromen-3-yl)(3-bromophenyl) methyl)-1,3-dimethylpyrimidine-2,4(1H,3H)-dione (4n). White solid; m.p. 245–247 °C; IR (KBr): 3405, 3210, 2924, 1673, 1665, 1617, 1489, 1445, 764 cm^{-1} ; ^1H NMR (400 MHz, $\text{DMSO}-d_6$) δ : 3.13 (s, 3H), 3.35 (s, 3H), 5.59 (s, 1H), 7.10–7.89 (m, 10H), 13.98 (s, 1H, OH); ^{13}C NMR (100 MHz, $\text{DMSO}-d_6$) δ : 28.74, 31.18, 36.17, 86.95, 104.94, 116.62, 117.31, 124.26, 124.85, 125.33, 126.54, 128.42, 128.94, 130.72, 132.90, 138.07, 150.52, 152.43, 155.64, 164.22, 164.50, 166.12; anal. calcd for $\text{C}_{22}\text{H}_{18}\text{BrN}_3\text{O}_5$: C, 54.56%; H, 3.75%; N, 8.68%. Found: C, 54.65%; H, 3.87%; N, 8.79%.

4. Conclusions

In conclusion, we reported an efficient method for the synthesis of chromenpyrimidines using the $\text{Co}_3\text{O}_4/\text{NiO}@G\text{QD}@SO_3\text{H}$ nanocomposite as a superior catalyst under reflux conditions. The new catalyst was characterized *via* FT-IR, SEM, XRD, EDS, TGA, BET and VSM. The current method provides obvious advantages, including environmental friendliness, short reaction time, reusability of the catalyst, low catalyst loading and simple workup procedure.

Conflicts of interest

There are no conflicts to declare.



Acknowledgements

The authors acknowledge a reviewer who provided helpful insights. The authors are grateful to University of Kashan for supporting this work by grant no.: 159196/XXI.

References

- 1 G. M. Ziarani, N. H. Nasab and N. Lashgari, *RSC Adv.*, 2016, **6**, 38827–38848.
- 2 R. S. Keri, K. M. Hosamani, R. V. Shingalapuri and M. H. Hugar, *Eur. J. Med. Chem.*, 2010, **45**, 2597–2605.
- 3 U. S. Rai, A. M. Isloor, P. Shetty, A. M. Vijesh, N. Prabhu, S. Isloor, M. Thiageeswaran and H. K. Fun, *Eur. J. Med. Chem.*, 2010, **45**, 2695–2699.
- 4 S. V. Laxmi, B. S. Kuarm and B. Rajitha, *Med. Chem. Res.*, 2013, **22**, 768–774.
- 5 N. R. Emmadi, K. Atmakur, C. Bingi, N. R. Godumagadda, C. G. Kumar and J. B. Nanubolu, *Bioorg. Med. Chem. Lett.*, 2014, **24**, 485–489.
- 6 A. A. Abu-Hashem and M. M. Youssef, *Molecules*, 2011, **16**, 1956–1972.
- 7 C. Sun, C. Chen, S. Xu, J. Wang, Y. Zhu, D. Kong, H. Tao, M. Jin, P. Zheng and W. Zhu, *Bioorg. Med. Chem.*, 2016, **24**, 3862–3869.
- 8 N. R. Kamdar, D. D. Haveliwala, P. T. Mistry and S. K. Patel, *Med. Chem. Res.*, 2011, **20**, 854–864.
- 9 T. P. Selvam, C. R. James, P. V. Dniandev and S. K. Valzita, *Res. Pharm.*, 2012, **2**, 01–09.
- 10 G. Basumatary, R. Mohanta and G. Bez, *Catal. Lett.*, 2019, **149**, 2776–2786.
- 11 G. Brahmachari, M. Mandal, I. Karmakar, K. Nurjamil and B. Mandal, *ACS Sustainable Chem. Eng.*, 2019, **7**, 6369–6380.
- 12 S. Abdolmohammadi, S. Balalaie, M. Barari and F. Rominger, *Comb. Chem. High Throughput Screening*, 2013, **16**, 150–159.
- 13 R. Bharti and T. Parvin, *Synth. Commun.*, 2015, **45**, 1442–1450.
- 14 R. Bharti and T. Parvin, *RSC Adv.*, 2015, **5**, 66833–66839.
- 15 X. T. Zheng, A. Ananthanarayanan, K. Q. Luo and P. Chen, *Small*, 2015, **11**(14), 1620–1636.
- 16 B. Senel, N. Demir, G. Büyükköroğlu and M. Yildiz, *Saudi Pharm. J.*, 2019, **27**, 846–858.
- 17 M. J. Molaie, *RSC Adv.*, 2019, **9**, 6460–6481.
- 18 T. F. Yeh, C. Y. Teng, S. J. Chen and H. Teng, *Adv. Mater.*, 2014, **26**, 3297–3303.
- 19 F. Xi, J. Zhao, C. Shen, J. He, J. Chen, Y. Yan, K. Li, J. Liu and P. Chen, *Carbon*, 2019, **153**, 127–135.
- 20 Y. Wang, Y. Shao, D. W. Matson, J. Li and Y. Lin, *ACS Nano*, 2010, **4**, 1790–1798.
- 21 Q. Li, S. Zhang, L. Dai and L. S. Li, *J. Am. Chem. Soc.*, 2012, **134**, 18932–18935.
- 22 A. L. M. Reddy, A. Srivastava, S. R. Gowda, H. Gullapalli, M. Dubey and P. M. Ajayan, *ACS Nano*, 2010, **4**, 6337–6342.
- 23 M. T. Hasan, R. Gonzalez-Rodriguez, C. Ryan, K. Pota, K. Green, J. L. Coffey and A. V. Naumov, *Nano Res.*, 2019, **12**, 1041–1047.
- 24 F. Temerov, A. Beliaev, B. Ankudze and T. T. Pakkanen, *J. Lumin.*, 2019, **206**, 403–411.
- 25 S. Zhu, Y. Song, X. Zhao, J. Shao, J. Zhang and B. Yang, *Nano Res.*, 2015, **8**, 355–381.
- 26 D. Qu, M. Zheng, J. Li, Z. Xie and Z. Sun, *Light: Sci. Appl.*, 2015, **4**, 364–371.
- 27 S. Sajjadi, A. Khataee, R. D. C. Soltani and A. Hasanazadeh, *J. Phys. Chem. Solids*, 2019, **127**, 140–150.
- 28 Y. Du and S. Guo, *Nanoscale*, 2016, **8**, 2532–2543.
- 29 Y. Yan, J. Gong, J. Chen, Z. Zeng, W. Huang, K. Pu, J. Liu and P. Chen, *Adv. Mater.*, 2019, **31**, 1808283–1808305.
- 30 M. Li, T. Chen, J. J. Gooding and J. Liu, *ACS Sens.*, 2019, **4**, 1732–1748.
- 31 Z. Wang, H. Zeng and L. Sun, *J. Mater. Chem. C*, 2015, **3**, 1157–1165.
- 32 E. Hu, X. Y. Yu, F. Chen, Y. Wu, Y. Hu, X. Wen and D. Lou, *Adv. Energy Mater.*, 2018, **8**, 1702476–1702483.
- 33 E. Hu, J. Ning, D. Zhao, C. Xu, Y. Lin, Y. Zhong, Z. Zhang, Y. Wang and Y. Hu, *Small*, 2018, **14**, 1704233–1704241.
- 34 E. Hu, Y. Feng, J. Nai, D. Zhao, Y. Hu, X. Wen and D. Lou, *Energy Environ. Sci.*, 2018, **11**, 872–880.
- 35 Q. Li, W. Lu, Z. Li, J. Ning, Y. Zhong and Y. Hu, *Chem. Eng. J.*, 2020, **380**, 122544–122552.
- 36 E. Hu, J. Ning, B. He, Z. Li, C. Zheng, Y. Zhong, Z. Zhang and Y. Hu, *J. Mater. Chem. A*, 2017, **5**, 2271–2279.
- 37 D. Qu, M. Zheng, P. Du, Y. Zhou, L. Zhang, D. Li, H. Tan, Z. Zhao, Z. Xie and Z. Sun, *Nanoscale*, 2013, **5**, 12272–12277.
- 38 K. Li, J. Chen, Y. Yan, Y. Min, H. Li, F. Xi, J. Liu and P. Chen, *Carbon*, 2018, **136**, 224–233.
- 39 N. Limchoowong, P. Sricharoen, Y. Areerob, P. Nuengmatcha, T. Sripakdee, S. Techawongstien and S. Chanthai, *Food Chem.*, 2017, **230**, 388–397.
- 40 F. Alemi-Tameh, J. Safaei-Ghomi, M. Mahmoudi-Hashemi and R. Teymuri, *Res. Chem. Intermed.*, 2016, **42**, 6391–6406.
- 41 J. Safaei-Ghomi, H. Shahbazi-Alavi and E. Heidari-Baghbahadorani, *RSC Adv.*, 2014, **4**, 50668–50677.
- 42 J. Safaei-Ghomi and H. Shahbazi-Alavi, *J. Saudi Chem. Soc.*, 2017, **21**, 698–707.

